Earthquake Engineering & Structural Dynamics
The Journal of the International Association for Earthquake Engineering

EARTHQUAKE ENGINEERING & STRUCTURAL DYNAMICS
Earthquake Engng Struct. Dyn. (2012)
Published online in Wiley Online Library (wileyonlinelibrary.com). DOI: 10.1002/eqe.2262

Bidirectional loading hybrid tests of square cross-sections of steel bridge piers

Ji Dang[1,*,†] and Tetsuhiko Aoki[2]

[1]*Kyoto University, Kyoto, Japan*
[2]*Aichi Institute of Technology, Toyota, Japan*

SUMMARY

Steel rectangular section columns with stiffened plates are commonly used for elevated highway bridges in the urban areas of Japan. The seismic design of bridge piers is usually performed by dynamic analysis in the horizontal direction using various independent directional seismic acceleration data. However, this simple treatment does not reflect the effect of bilateral loading as a structural response to inelastic interaction. In this study, unidirectional and bidirectional loading hybrid tests were conducted to examine the seismic response and performance of square cross-sections of steel bridge piers subjected to bidirectional seismic accelerations. Comparison of the results of unidirectional and bidirectional loading tests revealed that the maximum load is the same as the average of unidirectional loading in the NS and EW directions; however, the maximum response displacement and residual displacement increase in proportion with hard to soft ground types. Moreover, a modified seismic design is proposed considering these bidirectional loading effects. Copyright © 2012 John Wiley & Sons, Ltd.

Received 7 October 2011; Revised 29 August 2012; Accepted 31 August 2012

KEY WORDS: bidirectional loading; hybrid test; response behavior; steel bridge piers; square cross-section

1. INTRODUCTION

Elevated highways in urban areas are critical important structures because of their significant roles in rescue operations after earthquakes. Following the 1995 Kobe earthquake, Japanese seismic design specifications were revised [1]. In the present specifications, simplified design methods based on the response of structures under unidirectional horizontal earthquakes have been adopted. These methods conform to the assumption that there is a low probability of maximum seismic accelerations acting on structures simultaneously from two directions.

However, it may be difficult to capture the actual three-dimensional earthquake ground motions and structural responses by using simplified unidirectional loading-based methods. Even if the effect of vertical acceleration is negligible, a proper structure design should include the bidirectional horizontal loading effects because of strong ground motions.

Bidirectional quasistatic loading tests were performed by Watanabe *et al.* [2] that employed test specimens of a relatively small 150 mm × 100 mm cross-section of an electronically welded cold-formed rectangular steel tube with low residual stress. Moreover, Aoki *et al.* [3] conducted quasistatic cyclic loading tests for relatively large 450 mm × 450 mm specimens with rectangular welded sections composed of stiffened steel plates. The specimens were bidirectionally loaded under seven different loading patterns in the horizontal plane. It has been demonstrated by these tests that under diagonal direction linear loading, the maximum resistance load is similar to that under

*Correspondence to: Ji Dang, Kyoto University, Kyoto, Japan.
†E-mail: dang.ji.3x@kyoto-u.ac.jp

principal-axis directional loading. However, under circular route loading, the strength of steel columns is reduced to nearly half of that of unidirectional loading. Goto *et al.* [4] also performed unidirectional quasistatic cyclic loading tests and bidirectional diamond route loading tests by using 300 mm × 300 mm steel rectangular welded section specimens. The tests showed that horizontal force capacity showed great reduction under bidirectional loading than that under unidirectional loading. Similar deterioration of capacity also has been observed from the bidirectional loading tests for reinforced concrete columns [5, 6].

These studies involved bidirectional loading tests under simplified loading patterns in the horizontal plane, such as circular, diamond, square, and elliptic, following quasistatic cyclic loading procedures. However, the response behavior under an actual seismic acceleration wave was not investigated in these experimental studies.

Hybrid test technology is a currently available standard test procedure used to obtain the seismic responses of structures. In a hybrid test, the seismic response of the entire structure is derived from time domain simulation and the nonlinear hysteretic behavior of bridge piers, for which complete numerical analysis remains difficult, can be obtained through laboratory loading tests. These two processes are combined online and are conducted simultaneously. On the basis of this procedure, Nagata *et al.* [7] performed unidirectional and bidirectional loading hybrid tests for a 150 mm × 100 mm rectangular steel tube. Although their research is a pioneering work on hybrid tests for steel members, the tested specimen was a small cross-section composed of electronically welded and cold-formed steel with round corners that had little residual stress or initial deformation of the component plates. Such steel tubes are generally used for building columns but not for constructing thin-walled bridge piers composed of welded stiffened plates. The test results of unidirectional and bidirectional loadings in north-to-south (NS) and east-to-west (EW) directions were compared using a Kobe earthquake record, namely, Japan Meteorological Agency (JMA). In addition, Goto *et al.* [8] conducted unidirectional and bidirectional loading hybrid tests by using four test specimens of 325 mm × 300 mm cross-sections with the same seismic data (JMA). In their research, the results of two unidirectional loading tests for the two types of specimens subjected to unidirectional loading by using the NS component of the JMA data were compared with the bidirectional loading test results. Moreover, the researchers successfully compared FEM analysis results to the test results.

Because these two studies, [7, 8], revealed the restricted part of the response behavior of steel piers under the bidirectional excitation of a single ground motion JMA data, insufficient test data are available for refining the seismic design for actual ground motion. In the Japanese seismic design specifications [1], three sets of seismic acceleration data were prepared that correspond to three different representative ground types: hard (GT1), medium (GT2), and soft (GT3); these data were obtained from Kobe Earthquake records and tuned in amplitude over the frequency distribution. Dynamic analysis of these data is recommended; however, analytical or test results obtained for each independent NS or EW unidirectional loading are also allowed.

Beam-element nonlinear response analysis for steel piers without consideration of deterioration has been conducted [9, 10], and discussions of the response difference of unidirectional versus bidirectional loading revealed that these differences were also dependent on the earthquakes even when the deterioration effect was not considered. Hence, it is obviously important to clarify the nonlinear response behavior, of steel piers under bidirectional seismic loads with detailed loading tests by using at least these three sets of seismic data for the various ground types. Therefore, this study includes the following objectives:

(1) Obtain the seismic response behavior of steel piers under actual horizontal bidirectional loading conditions for the three ground types.
(2) Clarify the difference between the test results of bidirectional and unidirectional loadings by comparing these test data.
(3) Discuss the seismic design for steel piers under bidirectional loading conditions, although the test data are still insufficient to establish rational seismic design criteria.

In this study, two groups of unidirectional and bidirectional loading hybrid tests were conducted. The first group used identical test piers with the three different sets of seismic acceleration data specified in the Japanese seismic design specifications. The second group applied the same seismic motion (medium ground type GT2) but used three types of test specimens with different width-to-thickness parameters R_F.

DOI: 10.1002/eqe

2. TEST PROGRAMS AND TEST PROCEDURE

2.1. Test specimens

The side views and cross-sections of the test specimens are illustrated in Figure 1. All test pier specimens were prepared from 450 mm × 450 mm stiffened square cross-sections, and the plate thickness was 6 mm; the cross-section of vertical stiffeners was 6 mm × 55 mm. The plates were composed of SM490 steel with nominal yield strength of 325 N/mm^2. The three types of test specimens have different width-to-thickness ratios because of their differences in diaphragm intervals. As shown in Figure 1, all specimens were stiffened by diaphragms at intervals of 450 mm along a pier height of $h = 2.4$ m. Moreover, from the bottom to a height of 0.9 m, D150 specimens were stiffened by six diaphragms at intervals of 150 mm, and D225 specimens were stiffened by four diaphragms at intervals of 225 mm. The geometric sizes and properties of the test pier specimen cross-sections are listed in Table I. The width-to-thickness ratios R_R, R_F, and the slenderness parameter λ are defined by the following equations [11]:

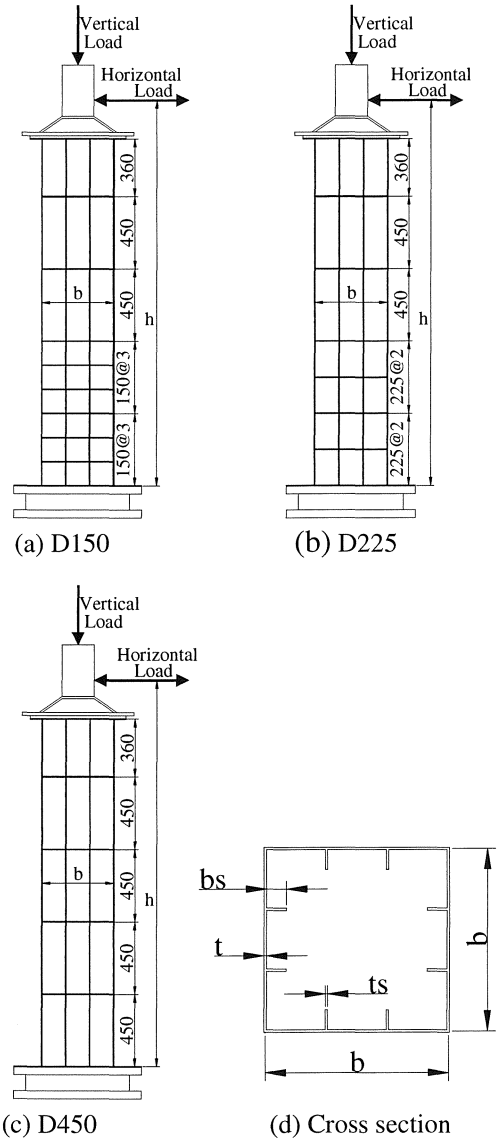

Figure 1. Side view (a) to (c) and cross-section (d) of test specimens.

DOI: 10.1002/eqe

Table I. Parameters of test specimens.

		D450	D225	D150
Height	h (mm)		2400	
Steel grade			SM490	
Plate width	b (mm)		450	
Plate thickness	t (mm)		6	
Section area	A (cm^2)		133	
Lib width	bs (mm)		55	
Lib thickness	ts (mm)		6	
Diaphragm interval	D (mm)	450	225	150
Second moment	I (cm^4)		4.06×10^4	
Width to thickness parameter	R_R		0.517	
Width to thickness parameter	R_F	0.353	0.178	0.119
Width to length parameter	λ		0.344	
Width to length parameter of stiffener	λs	0.388	0.184	0.129
Stiffener relative stiffness	γ/γ^*	2.49	10.5	26.7

$$R_R = \frac{b}{t}\sqrt{\frac{\sigma_y}{E}\frac{12(1-\nu^2)}{\pi^2 k_R}} \tag{1}$$

$$R_F = \frac{b}{t}\sqrt{\frac{\sigma_y}{E}\frac{12(1-\nu^2)}{\pi^2 k_F}} \tag{2}$$

$$\lambda = \frac{2h}{r}\frac{1}{\pi}\sqrt{\frac{\sigma_y}{E}} \tag{3}$$

$$k_F\begin{cases} \dfrac{(1+\alpha^2)^2 + n\gamma_1}{\alpha^2(1+n\delta_1)} & (\alpha \leqslant \alpha_0) \\ \dfrac{2(1+\sqrt{1+n\gamma_1})}{1+n\delta_1} & (\alpha > \alpha_0) \end{cases} \tag{4}$$

Here, α is the aspect ratio of the stiffened plate (0.3, 0.5, and 1 for D150, D225, and D450, respectively); α_0 is the critical aspect ratio (3.3); γ_1 is the rigidity ratio of the longitudinal stiffener (38); δ_1 is the cross-sectional ratio of one longitudinal stiffener (0.12) ; b is the plate width; t is the plate thickness; σ_y is the yield strength of the plate; E is the Young's modulus; v is the Poisson's ratio; n is the number of subpanels (3); r is the radius of gyration of the cross-section; h is the pier height; k_R is the buckling coefficient for R_R ($4n^2$) and k_F: buckling coefficient for R_F (Equation (4)).

For the three types of specimens, R_F changes from 0.353 to 0.119, whereas R_R and the slenderness parameter λ are kept constant at 0.517 and 0.344, respectively.

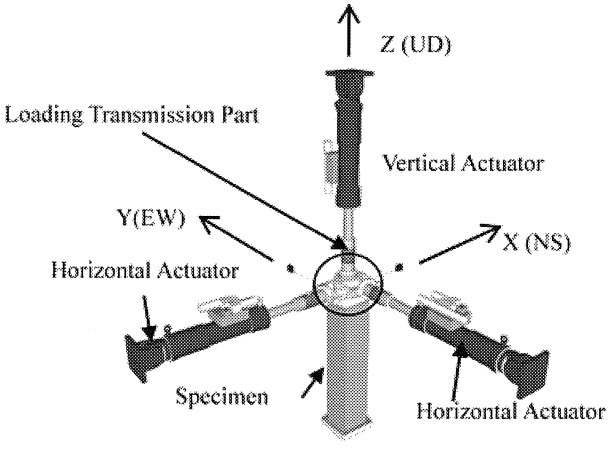

Figure 2. Loading system.

DOI: 10.1002/eqe

2.2. *Loading and measuring system*

Three 1000 kN actuators were set in the two orthogonal horizontal directions and the vertical direction, as shown in Figure 2. The axes of the three actuators were along the Cartesian coordinates *X*, *Y*, and *Z*, and their origin point was *O*, which coincides with the center of mass of bridge superstructure. Photo 1 (a) shows the side view of the loading system. A special loading apparatus, as illustrated in Figure 3 and Photo 1(b), was developed to move freely in three-dimensional rotation and shifting.

The system for measuring load and displacement consisted of three load cells (Ac_1, Ac_2, and Ac_3) located directly at the end of the actuators, and three sets of displacement transducers (DTs).

The first set of DTs had two high-precision string-pull-type digital signal DTs (D_1 and D_2) for measuring the horizontal displacement of the loading point. D_1 and D_2 were arranged on opposite sides of the two actuators. Because direct measurement is difficult for the displacements of the loading point *O*, which was located inside the three-axial rotating loading apparatus, the ends of the strings of D_1 and D_2 were connected to points *A* and *B*, 300 mm from the loading point *O* in the NS and EW directions, respectively (Figure 4(a)). The horizontal plane encompassing points *A*, *B*, and *O* is referred to as the measuring plane in this study and is indicated in Figure 4(a). Moreover, two analogue string-pull-type DTs, C_9 and C_{10}, were also arranged parallel to D_1 and D_2, respectively, and were connected to the corner of the measuring plane to measure its rotation angle around axis *Z*.

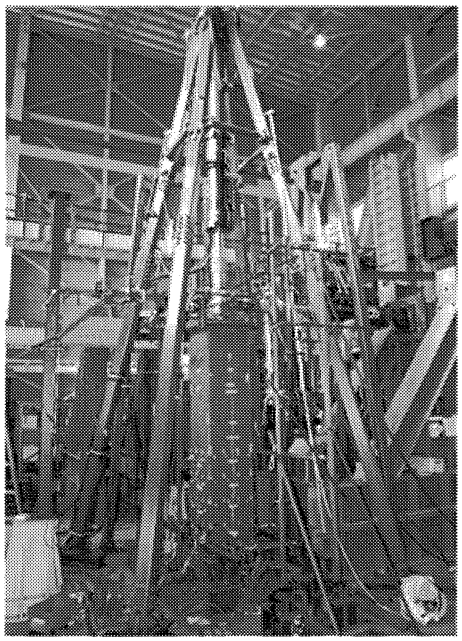

(a) Side view of loading system

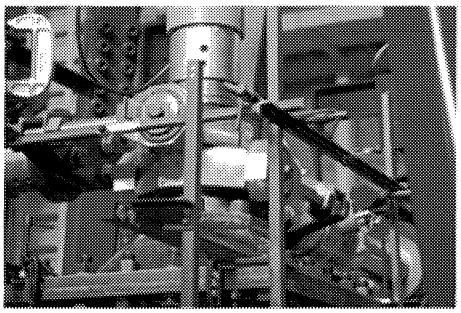

(b) The transmission part

Photo 1. Loading system: (a) side view of loading system and (b) the transmission part.

DOI: 10.1002/eqe

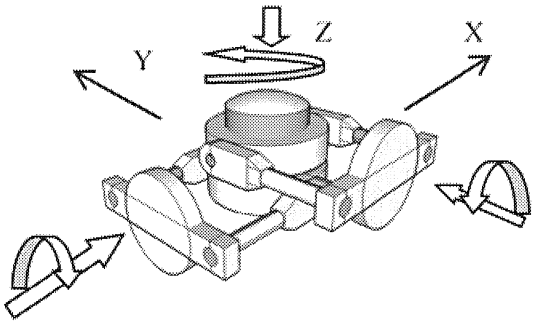

Figure 3. Loading apparatus.

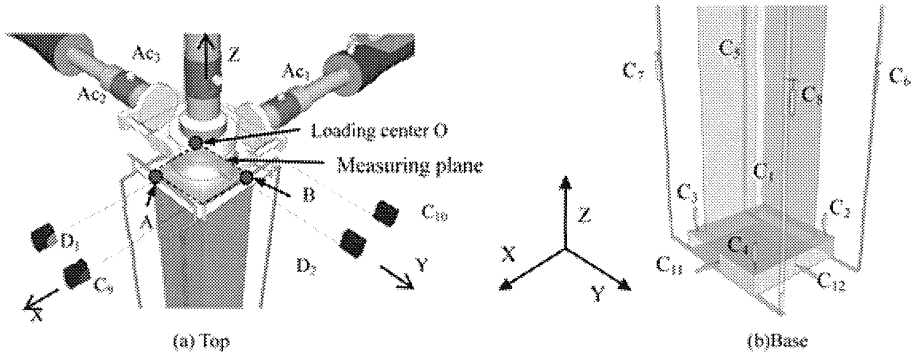

Figure 4. Settings of meters.

The second set of DTs [C_5–C_8 in Figure 4(b)] was set along the vertical sliding rods placed at the four corners of the specimen; these DTs measured the rotation angles of the measuring plane about the horizontal axes X and Y.

The third set of DTs (C_1–C_4) was used to measure the tilt angles of the pier base along axes X and Y. The C_{11} and C_{12} DTs were located at the bottom to measure the horizontal shift, as shown in Figure 4(b).

2.3. *Static cyclic loading test in the horizontal unidirection*

Prior to hybrid testing, six static cyclic unidirectional loading tests were performed. Pier specimens D150, D225, and D450 served to determine fundamental properties. For simplicity, a constant vertical load P (648 kN) was applied to all specimens. This value was determined from the axis load ratio of $P/P_y = 0.15$, where the yield vertical load $P_y = 4321$ kN was calculated from the nominal cross-sectional area ($A = 133\,\text{cm}^2$) of the pier and the nominal yield stress of the steel plate (σ_y= 325 MPa). The yield displacement δ_0 of a test pier is defined as the measured horizontal displacement when the strain at the bottom of the pier reaches the yield strain of tensile coupon tests. The horizontal load corresponding to the yield displacement δ_0 is defined as the yield load H_0.

2.4. *Hybrid test under unidirectional and bidirectional loading*

2.4.1. Test programs. In unidirectional and bidirectional horizontal loading tests, three sets of earthquake acceleration records from JMA, Japan Railway at Takatori (JRT), and Port-Island Kobe Bridge (PKB) [1] were used that correspond to the three different ground types: GT1 (hard), GT2 (medium), and GT 3 (ground). Each set of the seismic records contained NS and EW directional acceleration time history data.

Dynamic analysis was performed by using the physical properties of the full-size bridge pier identified from that of the scaled-size specimen following similarity rules under actual seismic acceleration as the simulation part of the hybrid test. The laboratory loading, as the experimental part, was conducted simultaneously by using a model specimen with the scale factor $S = 4$, which is

DOI: 10.1002/eqe

one-fourth the size of the actual bridge pier [14]. Single-degree-of-freedom and two-degrees-of-freedom models were used for the unidirectional and bidirectional loading tests, respectively. All tests shared the same superstructure mass in the simulation part and the same constant vertical load in the experimental part.

Test programs were planned to observe the manner in which bearing capacity decreases and response displacement changes under various bidirectional horizontal earthquake excitations or different component plate rigidities under the following conditions:

(1) Test Program 1: Input three different seismic acceleration data to the same bridge pier model D225 (test cases E1, E2, and E3 in Table II).
(2) Test Program 2: Input the seismic acceleration data (JRT) for GT2 to the three bridge pier model types, D150, D225, and D450, with different width-to-thickness ratios (test cases R1, R2, and R3 in Table II).

Test case R2 is identical to test case E2. In each test case, the responses of a bridge pier model under a set of earthquake records that contain both NS direction and EW direction acceleration components were measured in one bidirectional loading hybrid test and in two unidirectional loading hybrid tests using NS or EW direction components, respectively. Therefore, a total of 15 test specimens were used for unidirectional and bidirectional loading hybrid tests in this study. The test programs are listed in Table II.

Mass m (1058 t) corresponding to the specimen vertical load P (648 kN) was determined by the scale factor S (4) and gravitational acceleration ($g = 9.8\ \mathrm{m/s^2}$). In the actual primary seismic design [1], the safety factor v for each ground type is determined by the following equation:

$$v\left(P/P_y + M_0/M_y\right) = 1 \tag{5}$$

where M_0 ($k_h hW$) is the seismic moment determined by the design seismic coefficient k_h, which is defined as 0.2, 0.25, and $0.3g$ for GTs 1, 2, and 3, respectively. Here, W is the gravity of the superstructure. Therefore, the target piers have different safety factors of v = 1.49, 1.24, and 1.07 for GTs 1, 2, and 3, respectively, when using the constant axis load ratio P/P_y = 0.15.

The initial stiffness k_0 (64.4 kN/mm) of a bridge pier was calculated from the scale factor S, yield displacement δ_0, and yield force H_0, where δ_0 and H_0 were obtained from static cyclic loading tests. The damping coefficient c (0.825 kNs/mm) was determined by $c = 2\zeta\sqrt{k_0 m}$, where the damping ratio ζ = 0.05 was applied in this study. The natural period T was calculated as approximately 0.8 s.

2.4.2. Protocol of displacement control. The equation for the dynamic analysis of the bidirectional loading hybrid test at step $n+1$ is represented as follows:

$$[M]\{a\}_{n+1} + [C]\{v\}_{n+1} + \{R\}_{n+1} = [M]\{a_g\}_{n+1} \tag{6}$$

where

$$[M] = \begin{bmatrix} m & 0 \\ 0 & m \end{bmatrix},\ [C] = \begin{bmatrix} c & 0 \\ 0 & c \end{bmatrix},\ \{R\}_{n+1} = \begin{Bmatrix} R_x \\ R_y \end{Bmatrix}_{n+1},\ \{a\}_{n+1} = \begin{Bmatrix} a_x \\ a_y \end{Bmatrix}_{n+1},\ \{v\}_{n+1} = \begin{Bmatrix} v_x \\ v_y \end{Bmatrix}_{n+1},\ \{a_g\}_{n+1} = \begin{Bmatrix} a_{g,x} \\ a_{g,y} \end{Bmatrix}_{n+1}$$

Table II. Test programs.

Specimen type	R_F	Earthquake input (Ground type)		
		JMA(I)	JRT(II)	PKB(III)
D150	0.119		R1	
D225	0.178	E1	E2/R2	E3
D450	0.353		R3	

DOI: 10.1002/eqe

Here, R represents the bidirectional horizontal restoring force of the actual bridge pier, $\{a\}$ and $\{v\}$ are acceleration and velocity vectors of the gravity-centered mass point O, respectively, and $\{a_g\}$ is the seismic acceleration vector. Suffixes x and y indicate the NS and EW directions, respectively. The response is calculated using the well-known Newmark's β method (β = 1/6).

2.5. *Modification of measured displacement and load for bidirectional tests*

In three-axial loading tests, it is important to determine the correct values of load and displacement at the center mass of the modeled pier in the three coordinate axes. Originally, loads and displacements were measured along the orthogonal lines passing through point O. However, during the loading process, the initial measuring lines from fixed points to the center of mass O become oblique to the Cartesian coordinate axes. Therefore, it was necessary to modify the measured displacements and loads to consider the effect of the tilt angle of the measuring plane at the pier top and the rotation angle of the specimen's base.

Modifications of the measurement have been performed according to the following three steps during the loading process:(1) Modification of displacement because of the rotation of the measuring plane at the pier top.(2) Modification of displacement because of the rotation of the pier base.(3) Modification of measured loads.

Details of this process are demonstrated in [12, 13].

3. TEST RESULTS AND CONSIDERATIONS

3.1. *Static cyclic tests results*

The load–displacement hysteretic curves obtained from the six static cyclic tests are illustrated in Figure 5. The yield displacement δ_0, yield load H_0, elastic stiffness k_0, peak load H_m, and displacement of peak load δ_m were obtained from the tests and are listed in Table III. The average values of δ_0 and H_0 and those of δ_m and H_m obtained from the two tests for the same specimen types are listed in the table in the left-hand cells beside the direct values of these tests. Henceforth,

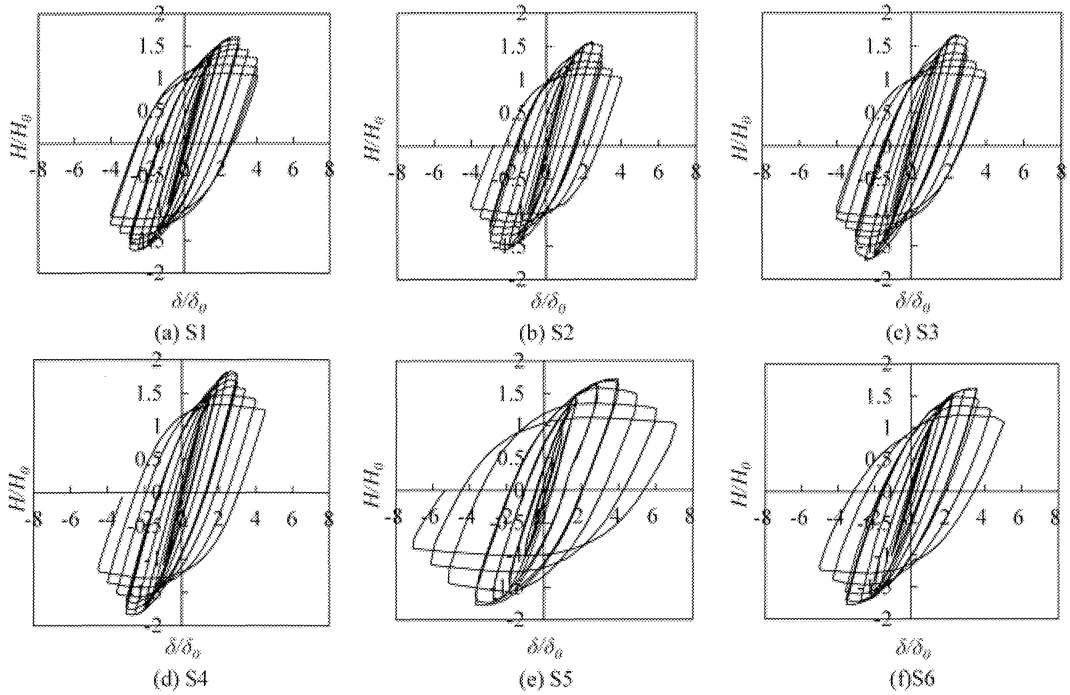

Figure 5. Hysteretic curves of static cyclic tests.

DOI: 10.1002/eqe

Table III. Static cyclic test results.

Test code	Specimen type	R_F	δ_0 (mm)		H_0 (kN)		k_0 (kN/mm^2)	δ_m (mm)	(δ_m/δ_0)	H_m (kN)	(H_m/H_0)
S1	D150	0.119	15.0	14.8	252	242	16.8	35.2	39.1	394	395
S2			14.6		232		15.9	42.9	(2.64)	396	(1.63)
S3	D225	0.178	16.0	15.0	243	234	15.2	39.8	38.5	407	397
S4			14.0		224		16.0	37.2	(2.57)	386	(1.70)
S5	D450	0.353	11.5	12.4	200	202	17.4	43.8	42.8	347	345
S6			13.2		203		15.3	41.7	(3.46)	342	(1.71)

the average values of δ_0 and H_0 are used to normalize displacement and force. The normalized values of δ_m and H_m, δ_m/δ_0, and H_m/H_0, are listed in the table inside the parentheses. The values in Table III indicate that the peak load points (δ_m, H_m) are affected by the width-to-thickness ratio R_F, although D150 and D225 show nearly the same values. The values of H_m increase when the values of R_F decrease because of the diaphragms set at smaller intervals. However, displacement at the peak load point δ_m decreases with R_F, as expected. Local buckling developed at the constituent plates of specimens between the lowest diaphragms and the base plates. All specimens were loaded until severe damage accompanied with out-of-plane deformation occurred, as shown in Photo 2. Slight cracks along the welding in the corner of the cross-sections were also observed after the loading was complete.

3.2. Hybrid test results

The major results of both unidirectional and bidirectional hybrid loading tests, including the peak load H_m/H_0, maximum response displacement δ_{max}/δ_0, and residual displacement δ_r/δ_0 are listed in Table IV. The hysteretic curves obtained from the unidirectional and bidirectional loading hybrid tests are represented by broken and solid lines, respectively, in Figure 6 for the tests of test program

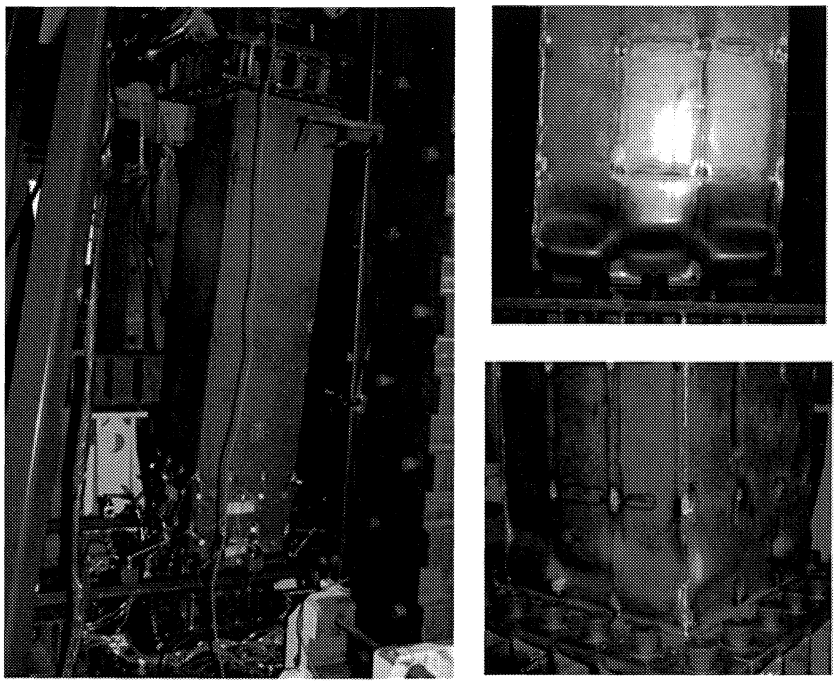

Photo 2. Failures of specimen observed after static cyclic loading (S1)

DOI: 10.1002/eqe

Table IV. Results of unidirectional and bidirectional loading hybrid tests.

Test program	Test case	Specimen type	RF	Earthquake (Ground type)	direction	H_{mu}/H_0	H_{mb}/H_0	H^*_{mb}/H_0	δ_{mu}/δ_0	δ_{mb}/δ_0	δ^*_{mb}/δ_0	δ_{ru}/δ_0	δ_{rb}/δ_0	δ^*_{rb}/δ_0
1	E1	D225	0.178	JMA(1)	NS	1.56	1.42	1.49	3.68	2.82	3.33	1.48	0.67	0.93
					EW	1.86	1.31		2.86	2.31		0.74	0.64	
	E2	D225	0.178	JRT(2)	NS	1.81	1.50	1.71	5.46	6.59	7.40	2.21	4.31	4.37
					EW	1.66	1.65		4.82	4.04		2.05	0.67	
	E3	D225	0.178	PKB(3)	NS	1.64	1.45	1.55	5.18	>12.8	15.8	2.93	12.2	15.1
					EW	1.58	1.11		8.04	>9.77		6.13	8.90	
2	R1	D150	0.119	JRT(2)	NS	1.65	1.35	1.52	5.13	>10.1	10.2	1.35	9.48	9.52
					EW	1.61	1.47		4.73	>4.69		1.59	0.94	
	R2	D225	0.178	JRT(2)	NS	1.81	1.50	1.71	5.46	6.59	7.40	2.21	4.31	4.37
					EW	1.66	1.65		4.82	4.04		2.05	0.67	
	R3	D450	0.353	JRT(2)	NS	1.72	1.65	1.91	8.09	>8.56	9.90	2.73	3.57	5.07
					EW	1.74	1.85		4.59	>6.41		0.78	3.58	

H^*_{mb}, δ^*_{mb}, andδ^*_{rb}: vector composed values of NS and EW components under bidirectional loading.

DOI: 10.1002/eqe

1 (E1, E2, and E3 in Table II) and in Figure 7 for the tests of test program 2 (R1, R2, and R3). The displacement time history curves obtained from the unidirectional and bidirectional loading hybrid tests are illustrated by broken and solid lines, respectively, in Figures 8 and 9 for the tests of program 1 and 2, respectively.

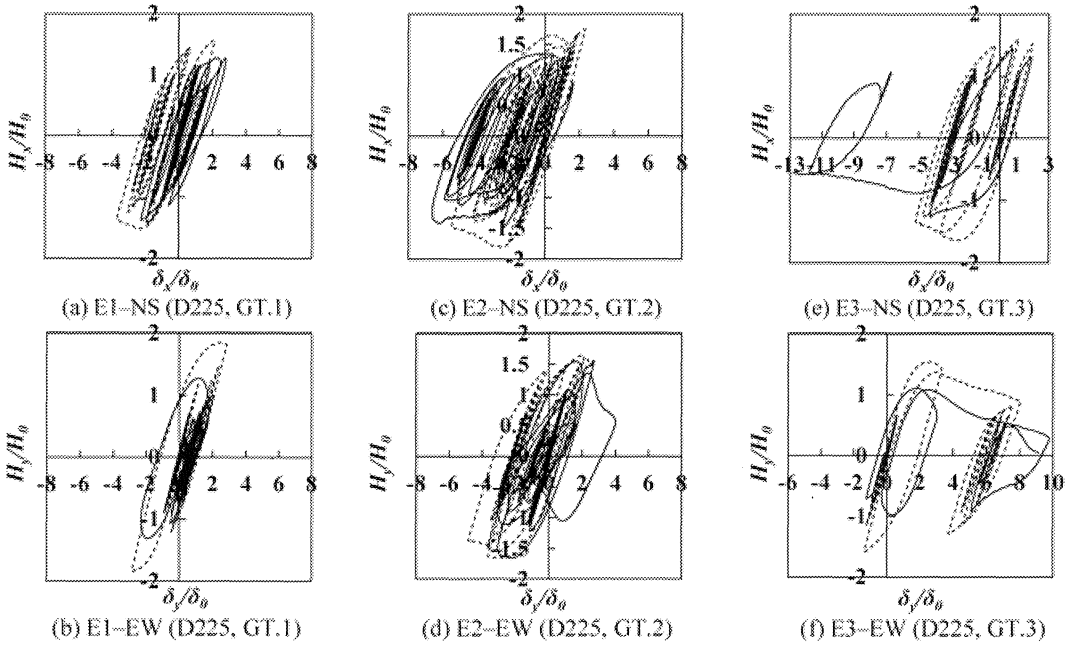

Figure 6. Hysteretic curves of test program 1, solid and dashed lines for bidirectional and unidirectional tests.

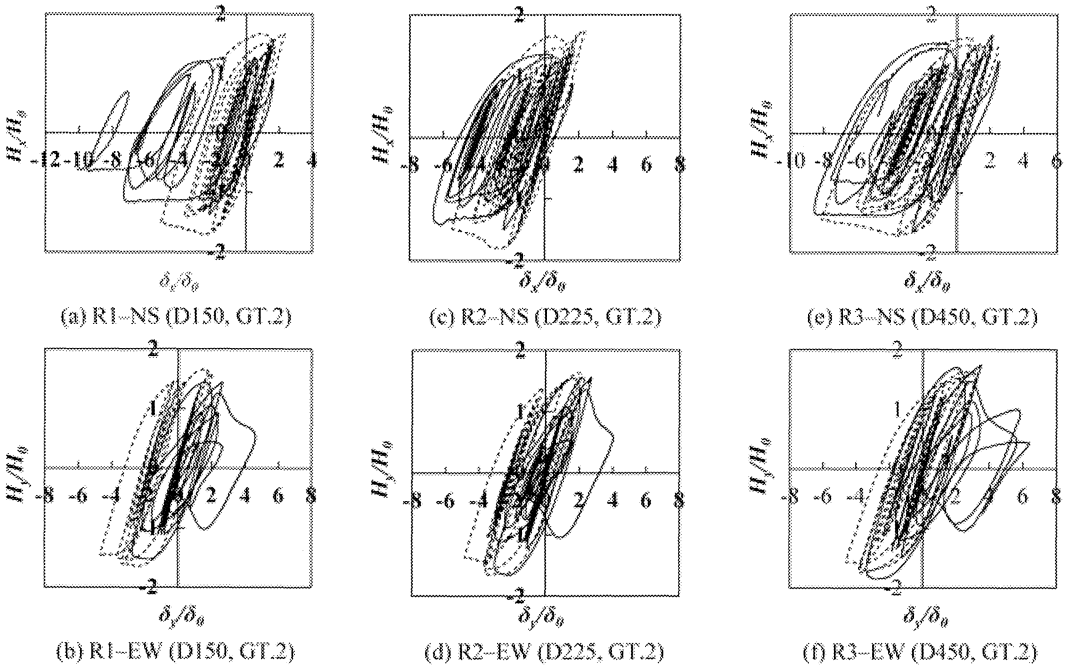

Figure 7. Hysteretic curves of test program 2, solid dashed lines for bidirectional and unidirectional tests.

DOI: 10.1002/eqe

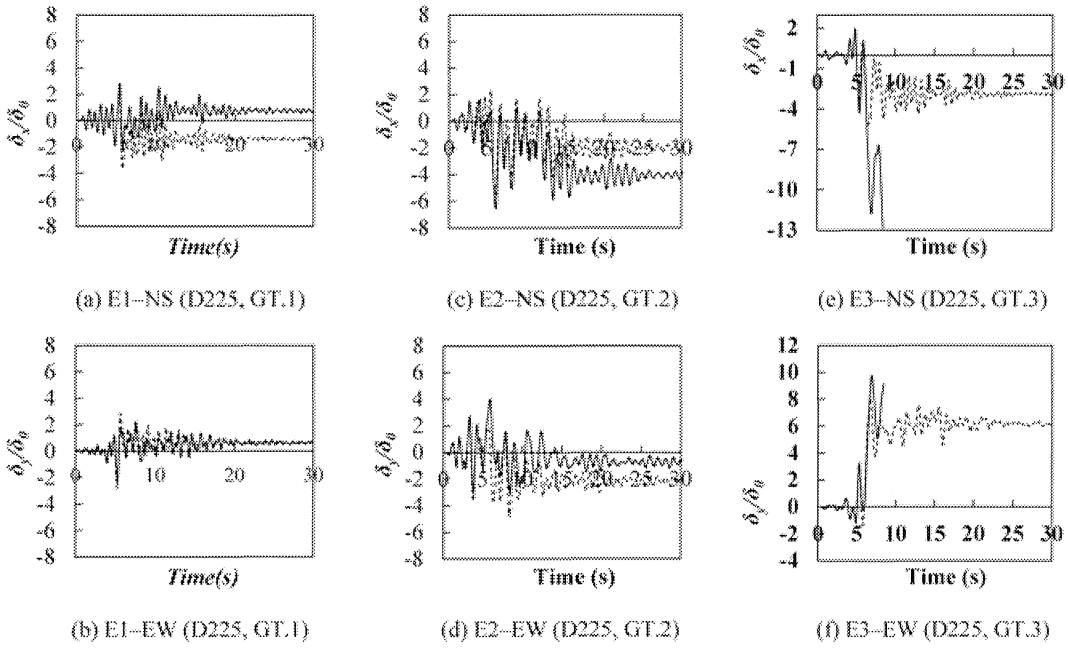

Figure 8. Displacement time history of the test program 1, solid and dashed lines for bidirectional and unidirectional tests.

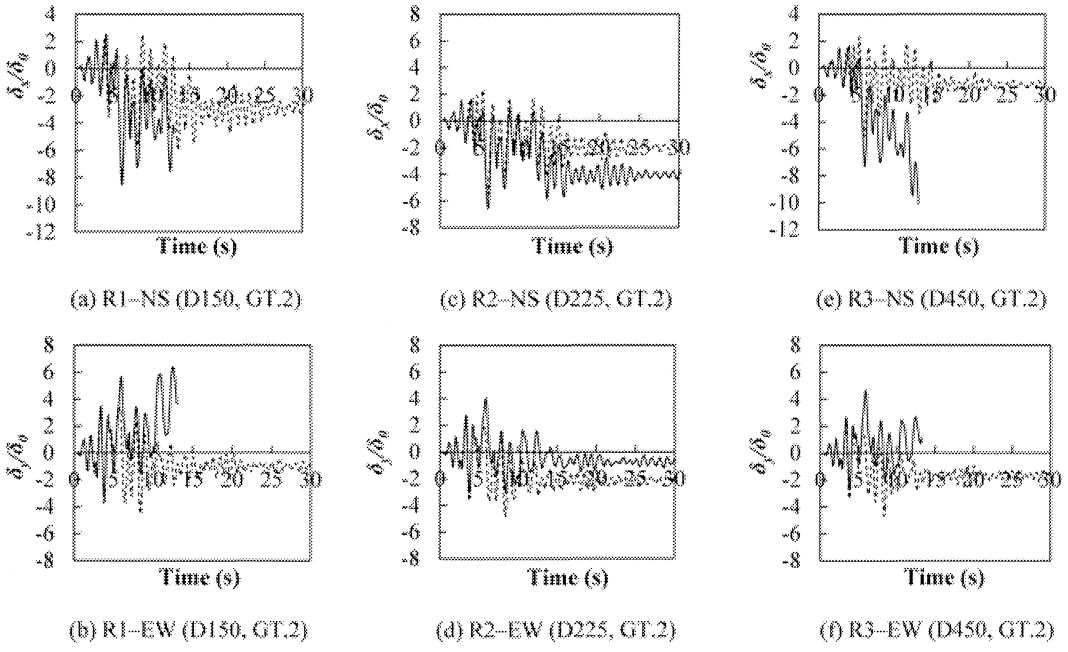

Figure 9. Displacement time history of the test program 2, solid and dashed lines for biunidirectional tests.

3.2.1. Hysteretic curves. Obvious expansion in displacement because of bidirectional loading compared with that because of unidirectional loading can be observed in Figure 6, particularly in the cases of E3-NS and E3-EW (Figures 6(e)–(f)). The maximum loads in the hysteretic curves for bidirectional loading showed extensive deterioration, except in the case of E2-EW. In the test cases R1-NS and R3-EW (Figures 7(a)–(f)), the piers for the bidirectional loading hybrid tests showed that a significant decrease in load resistance was accompanied by an increase in displacement.

DOI: 10.1002/eqe

3.3.2. Displacement time history. From the time history diagrams of the response displacement (Figures 8 and 9), maximum response displacement, and residual displacement because of bidirectional loading (solid lines) are generally larger than those because of unidirectional loading (broken lines).

In the cases of E3 (Figures 8(e) and (f)), R1 (Figures 9(a) and (b)), and R3 (Figures 9(e) and (f)), the center of response displacement oscillation gradually slid off the center of time axis because of bidirectional loading, which resulted in divergence. Therefore, the loading tests had to be stopped midway before the end of time history. These piers were considered as 'collapse' because of the low observed residual bearing capacity and extremely large displacement accompanied by significant local buckling and cracks, as shown in Photo 3. On the contrary, the unidirectional loading resulted in neither collapse nor divergence in the response displacement time history.

3.3.3. Tracks of response displacement in the horizontal plane. The bidirectional displacement tracks of the center of the mass point at the pier tops in the horizontal plane are shown in Figure 10, in which the vertical and horizontal axes indicate response displacement of the piers in the NS and EW directions, respectively. Figures 10(a)–(c) show the test results for test program 1. Comparison of these three graphs revealed that the shapes of the response displacement tracks change significantly when the ground motion changes. Figures 10(d)–(f) show the results of test program 2, in which the rigidity of specimens varied but the seismic input is the same one (GT.2). Only small changes in the displacement tracks can be observed among these three cases. In all figures, the displacement tracks are stretched because of bidirectional loading in the NW direction, whereas the tracks because of unidirectional loading remained within the circular-like area.

3.3.4. Tracks of loading in the horizontal plane. Bidirectional loading tracks in the horizontal plane are shown in Figure 11, in which the vertical and horizontal axes represent the horizontal force of the piers in the NS and EW directions, respectively. The solid lines in these figures, representing the results of bidirectional loading tests, exhibit circular-like forms. However, the broken lines, which represent the results for unidirectional loading, show a square-like form and generally envelope the circular-like bidirectional loading results regions. Accordingly, the superposition of horizontal forces

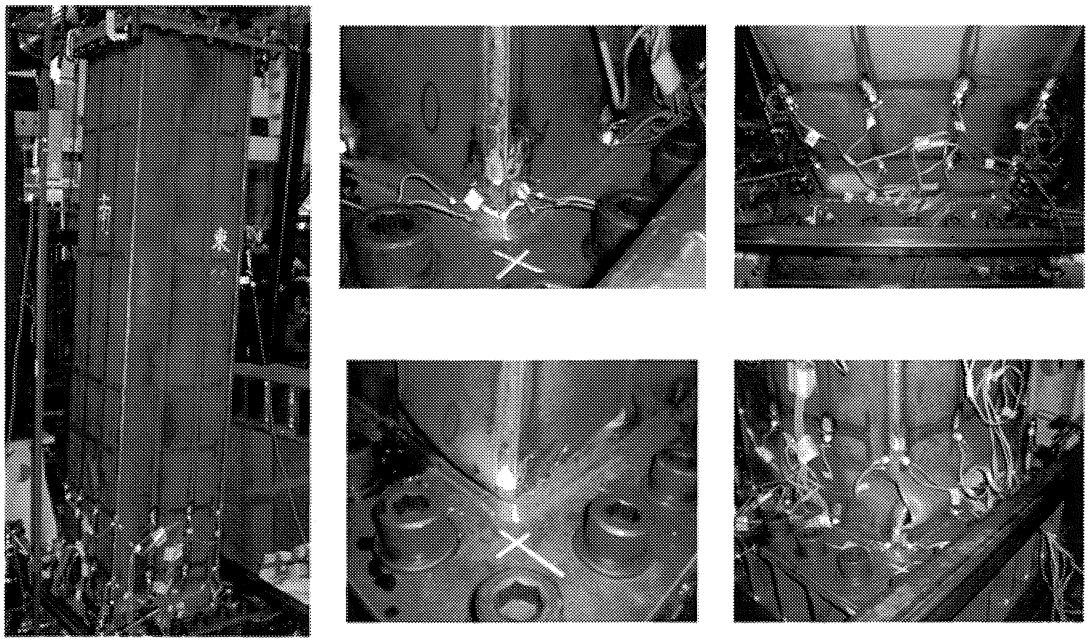

Photo 3. Failures because of bidirectional earthquake excitation (E3).

DOI: 10.1002/eqe

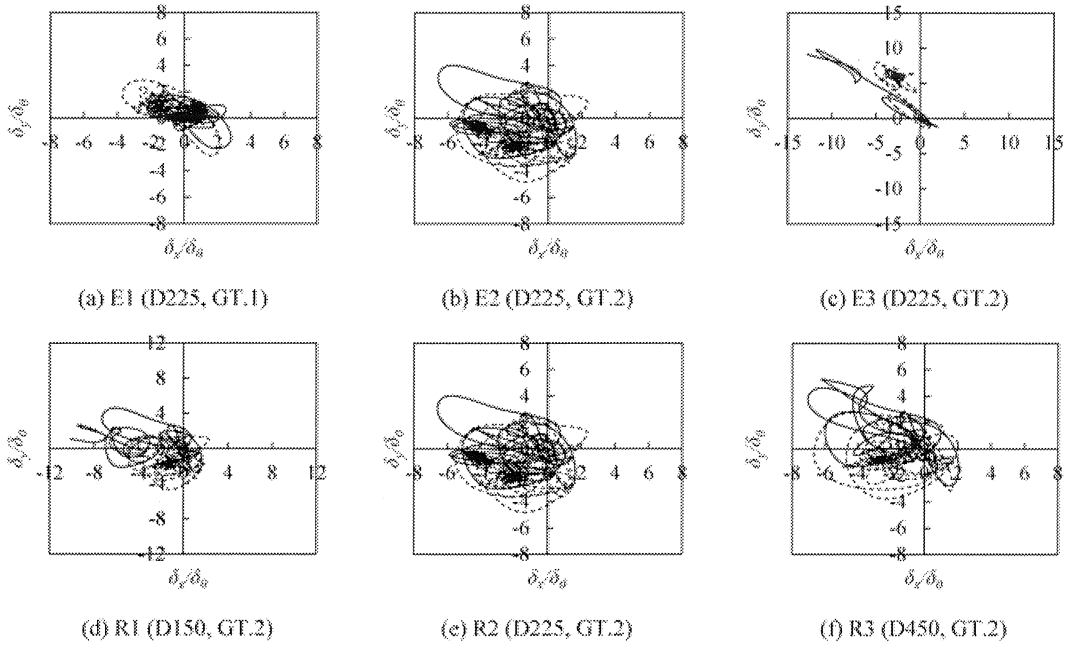

Figure 10. Response displacement tracks, solid and dashed lines for bidirectional and unidirectional tests.

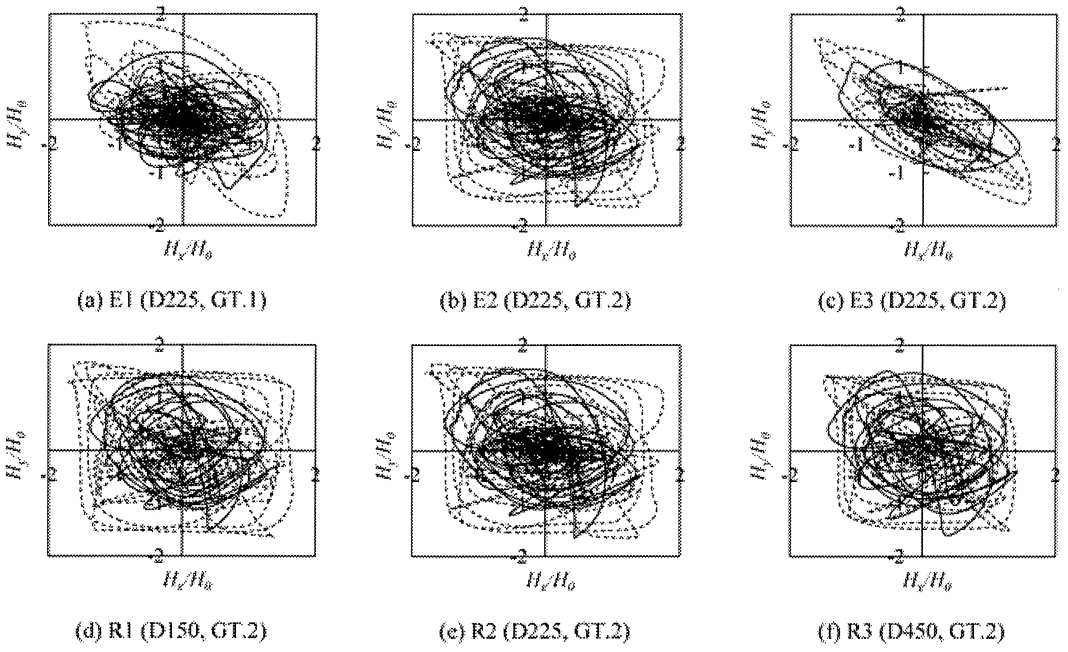

Figure 11. Horizontal force tracks, solid and dashed lines for bidirectional and unidirectional tests.

analyzed independently in the two orthogonal directions resulted in larger force tracks, leading to an overestimation of the hysteretic horizontal force of the actual three-dimensionally loaded steel piers.

3.3.5. Maximum load. Figure 12 compares the maximum loads $H_{mu\text{-}\mathrm{NS}}$ and $H_{mu\text{-}\mathrm{EW}}$ obtained from unidirectional loading and H^*_{mb} obtained from bidirectional loading. The maximum load H^*_{mb} represents horizontal force in oblique directions creating the maximum values, and is calculated as a

DOI: 10.1002/eqe

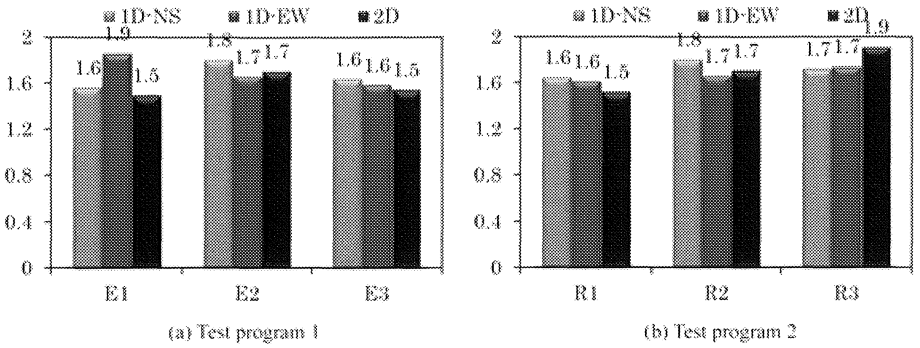

Figure 12. Maximum force H_{mb}/H_0 and H_{mu}/H_0.

vector composition of NS and EW components measured during the bidirectional loading process. Obviously, there is a minimal difference observed among these chart columns. The average maximum loads of NS and EW directions under unidirectional loading H^a_{mu} agrees well with the maximum loads H^*_{mb} under bidirectional loading, with a difference of less than 1%, although scatter in the data is observed.

3.3.6. Maximum displacement and residual displacement. Figure 13 compares the maximum displacement of unidirectional and bidirectional loadings, in which the two left-hand columns represent the NS and EW directional maximum displacements because of unidirectional loading and the right-hand column indicates the displacements because of bidirectional loading, which were calculated as vector compositions of NS and EW components.

It is clear from Figure 13(a), which shows the results of test program 1 for different ground types, that response displacement increases with hard to soft ground types. The average of the nondimensional maximum displacements δ^a_{mu}/δ_0 because unidirectional loading for E1, E2, and E3 are 3.3, 5.1, and 6.6, respectively, and the corresponding values because of bidirectional loading are 3.3, 7.4, and >15.8, respectively. Then, the ratio of the displacement because of bidirectional loading to that because of unidirectional loading also changes as 1.0, 1.5, and 2.4 for E1, E2, and E3, respectively. This result is important because it indicates that the response displacement caused by actual seismic oscillation cannot be adequately predicted by unidirectional loading tests or analysis.

From Figure 13(b), which shows the results of test program 2 using different piers, there is no significant difference among these specimens, except the case R3 in NS, but the average displacement because of bidirectional loading is 1.7 times of that because of unidirectional loading.

Figure 14 compares the residual displacement because of unidirectional and bidirectional loadings, in which the two left-hand columns list the results of unidirectional and the right-hand columns list the results of bidirectional loading tests. A similar tendency is observed in this figure as in the maximum response displacement shown in Figure 15, but the difference between unidirectional and bidirectional loadings is extended. The ratios of residual displacement because of bidirectional loading to that

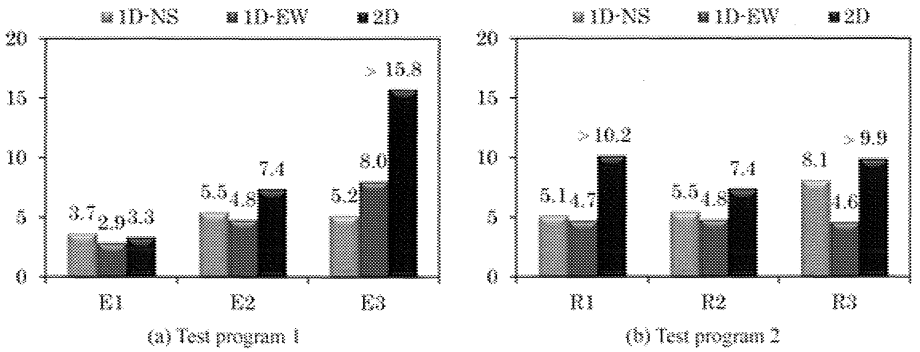

Figure 13. Maximum response displacement in unidirectional and bidirectional tests.

DOI: 10.1002/eqe

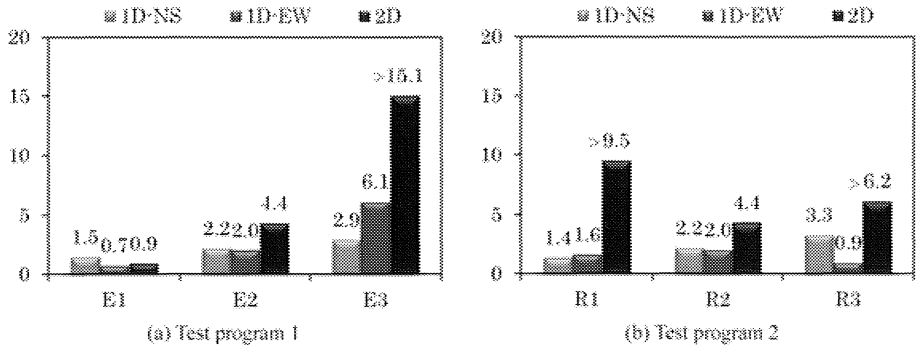

Figure 14. Residual displacement in unidirectional and bidirectional directional tests.

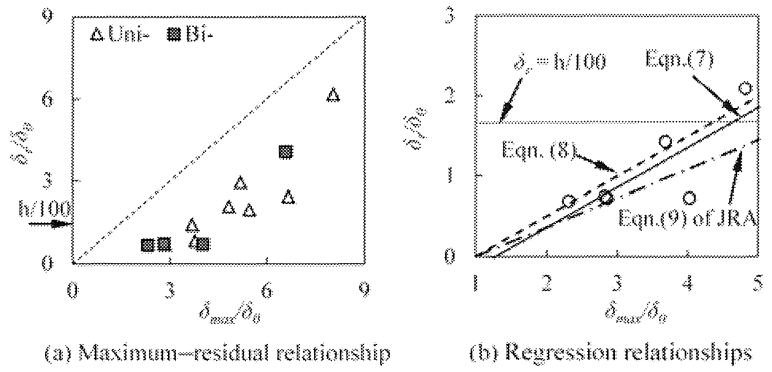

Figure 15. Relationship between the maximum and residual displacements.

because of unidirectional loading are 0.93, 2.05, and 3.46 for specimens E1, E2, and E3, respectively. The average residual displacement of bidirectional loading was 5.1 times that of unidirectional loading for test program 2. These results indicate that it is also inadequate to evaluate residual displacement based only on conventional unidirectional loading tests or analysis.

3.3.7. Relationship between maximum and residual displacement. Figure 15(a) shows the relationship between residual displacement (δ_{ru} and δ_{rb}) and maximum displacement (δ_{mu} and δ_{mb}), except for the results of the aforementioned 'collapsed' tests (E3, R1, and R3). The figure reveals that the plotted points for unidirectional and bidirectional loadings, indicated by Δ and ■, respectively, show nearly identical tendencies.

The limit of residual displacement for bridge piers is prescribed in the Japanese seismic design specifications [1] as less than 1/100 of the pier height, which corresponds to $\delta_r < 1.6\delta_0$ for test specimens of this study. To determine the relationship between residual and maximum displacements $\delta_r - \delta_{\max}$, test data $\delta_r < 3\delta_0$ were selected and plotted in Figure 15(b), from which the mean regression relationship, represented by solid lines in the figure, was obtained from the following linear equation:

$$\delta_r/\delta_0 = 0.50\delta_{\max}/\delta_0 - 0.65 \tag{7}$$

The standard deviation σ, which expresses the bandwidth of the data scatter around linear equation (7), is calculated as $\sigma = 0.64\delta_0$.

Because no residual displacement will remain in the region of $\delta_{\max} < \delta_0$, the regression line passing through the point (1, 0) on the horizontal axis can be recognized as the upper limit of the estimation of residual displacement. This line is expressed as Equation (8) and is indicated by a broken line in Figure 15(b). This line corresponds to $M + 0.44\,\sigma$, where M is mean value and σ is standard deviation.

DOI: 10.1002/eqe

$$\delta_r/\delta_0 = 0.5(\delta_{\max}/\delta_0 - 1) \tag{8}$$

In the design specifications [1], Equation (9) is proposed with the coefficients $C_R = 0.45$ and $r = 0.2$ for hollow steel piers, which is shown as a dotted line in Figure 15 (b).

$$\delta_r/\delta_0 = C_R(\delta_{\max}/\delta_0 - 1)(1 - r) \tag{9}$$

Equation (8) is considered to be a better estimation of the test data, which can be expressed in the form of Equation (9) with the coefficients $C_R = 0.625$ and $r = 0.2$.

3.3.8. Energy absorption capacity. The time history diagrams of energy absorption under unidirectional and bidirectional loadings are illustrated in Figure 16, which are defined as the accumulation of the product of the displacement increment $(\delta_{n+1} - \delta_n)$ and the horizontal force H_{n+1} using Equation (10), and are normalized by the unit elastic energy absorption $E_0 = H_0\delta_0/2$, where H_0 and δ_0 are the yield force and displacement, respectively.

$$E = \sum(\delta_{n+1} - \delta_n)H_{n+1} \tag{10}$$

Figure 16 shows that the energy absorption curves reached a plateau within the first 15 s. The final energy absorptions under bidirectional loading were calculated to be nearly the same as the sum of the energies in the NS and EW directions under unidirectional loading.

4. SEISMIC DESIGN CONSIDERATIONS

Conventional seismic design allows for the use of results obtained from unidirectional loading tests or analyses, as previously mentioned. From observations focused on the difference between the results of unidirectional and bidirectional loading hybrid tests, a more rational design treatment should be considered on the basis of major indices such as maximum resistance force, maximum response

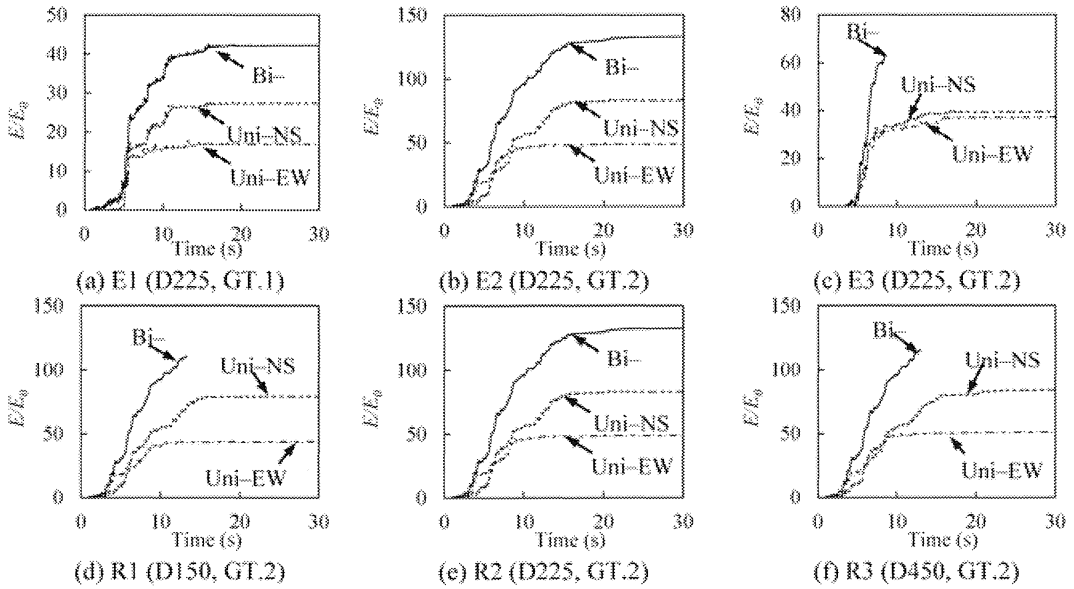

Figure 16. Energy absorption time history.

DOI: 10.1002/eqe

displacement, and residual displacement. It is preferable to modify a design method on the basis of previous conventional approaches to avoid unfamiliarity and complexity.

4.1. Maximum load

The average of the maximum load of the unidirectional loading test showed nearly the same value as that observed in bidirectional loading tests, and the insignificant differences can be ignored in practical design. Therefore, regarding the maximum resistance load under actual seismic bidirectional loading conditions, the average of conventional unidirectional loading results can be used even for different ground types.

4.2. Response maximum displacement

For steel bridge piers, the admissible displacement given in the seismic design specifications [1] is described as the displacement δ_{ma}, and it is the maximum load reached in repeated cyclic loading tests or analysis. In this study, δ_{ma}/δ_0 was obtained from cyclic loading tests as 2.9 (referred to as δ_m in Table III); the hybrid test results shown in Figure 15 revealed that nearly all results exceeded this admissible value. Therefore, the size of the pier section or the rigidity of the stiffened plate should be changed in line with the routine design procedure on the basis of the results obtained from unidirectional loading tests.

However, as shown in Figure 15, the response displacements because of bidirectional loading significantly exceeded this limit even more. Therefore, an adjustment is required to maintain safety after changing the unidirectional loading process. Assuming that the ratio of response displacement because of bidirectional loading to that because of unidirectional loading, which are 1.0, 1.5, and 2.4 for ground types 1, 2, and 3 for hard to soft ground, does not change during the control of constituent plates of piers, the following modification, corresponding to the various ground types, is proposed:

$$\delta^*_{ma} = \beta_m(i)\delta_{ma} \tag{11}$$

Here, δ^*_{ma} is a new admissible response displacement because of the bidirectional loading; δ_{ma} is the conventional admissible response displacement because of unidirectional loading; and $\beta_m(i)$ could be 1.0, 0.67, or 0.42 according to the ground type i (1, 2, or 3), which is the inverse of the previously mentioned ratio. Accordingly, the new admissible displacement δ^*_{ma} should be applied when the design based on the conventional unidirectional loading results is used. The results from test program 2 displayed in Figure 15(b) are included in the above modification of Equation (11), although the ratio of displacement because of bidirectional loading to that because of unidirectional loading presents scatter in some cases.

4.3. Residual displacement

The residual displacement shown in Figure 16 exhibits the same condition as the maximum response displacement shown in Figure 15 because of their linear relationship. The admissible residual displacement [1] is regulated as less than 1/100 of the pier height, which corresponds to $\delta_r < 1.6\delta_0$ for this test specimen, as previously mentioned. Comparing this value to that of the test results as shown in Figures 16(a) and (b) reveals that half of the results of unidirectional loading tests surpass this limit. Regarding the maximum response displacement, pier rigidity should be modified to maintain the regulation on the basis of the unidirectional loading test results or analysis. However, for the bidirectional loading condition, the limit criterion δ_{ra} should also be modified as follows:

$$\delta^*_{ra} = \beta_r(i)\delta_{ra} \tag{12}$$

where δ^*_{ra} is a new admissible displacement because of the bidirectional loading effect; δ_{ra} is the conventional admissible displacement; $\beta_r(i)$ is 1.0, 0.5, and 0.3 for ground type i (1, 2, and 3, respectively), which are the inverse of the previously mentioned ratio for the residual displacement.

DOI: 10.1002/eqe

As a result, the new admissible residual displacement δ_{ra}^{*} should be applied when the design based on conventional unidirectional loading results is used.

Although the response value of the residual displacement can be obtained by nonlinear dynamic simulation based on unidirectional loading, the accuracy of the previous methods is generally suspect in terms of residual displacement. Hence, the residual displacement should be checked by using the value evaluated against the maximum displacement because of the above Equation (8) or Equation (9) with parameters C_R= 0.625 and r = 0.2, respectively, to assess immediate emergency transit performance after an earthquake.

5. CONCLUSIONS

In this study, 15 hybrid loading tests were conducted by using welded square-sectional steel bridge pier models under unidirectional loading in the NS and EW directions alone and under simultaneous bidirectional loading. The seismic acceleration data for the three ground types specified in the Japanese seismic design specifications for road bridges were used as the input earthquake data. Test program 1 used three identical test specimens but different seismic records. Test program 2 used three types of test specimens with various diaphragm intervals but the same seismic record. The conclusions can be summarized as the following points:

(1) Obvious differences were observed in the hysteretic curves and response displacement time history curves under unidirectional and bidirectional loadings. For three of the five bidirectional loading tests, displacement divergence, and subsequent collapse of the specimens occurred, whereas all specimens in unidirectional loading tests remained stable.
(2) Nearly all displacement tracks because of bidirectional loading emerged on the horizontal plane extending in the NW direction, whereas the tracks because of unidirectional loading remained within a small circular region.
(3) The average of maximum loads in the NS and EW directions under unidirectional loading agreed well with those under bidirectional loading. Regarding the maximum load, the seismic design value obtained from the result of dynamic analysis because of conventional unidirectional loading can be used.
(4) The maximum response displacement under both unidirectional and bidirectional loadings increased in accordance with hard to soft ground types. The ratio of maximum response displacement because of bidirectional to unidirectional loading changed as 1.0, 1.5, and 2.4 for these ground types. For the seismic designs that consider the bidirectional loading effect, a modified admissible displacement method is proposed.
(5) Seismic design specification based solely on unidirectional loading test results such as those for displacement and force may lead to safety issues. Displacement differences between unidirectional and bidirectional loadings were significant depending on the ground motion input.
(6) The estimation equation of the residual displacement from the maximum response displacement was proposed for the data in the range $\delta_r < 2.0\delta_0$. For the current design equation specified in [1], the coefficients $C=0.65$ and $\gamma=0.2$ are adaptable, which is an accurate estimation that covers the upper bound for most data.
(7) Energy absorption under bidirectional loading can be estimated as the sum of the energies dissipated in the NS and EW directions under unidirectional loading.

REFERENCES

1. Japan Road Association. Design Specifications of Highway Bridges (Part V. Seismic Design) 2002.
2. Watanabe E, Sugiura K, and Oyawa WO. Effects of Multi–Directional Displacement Paths on the Cyclic Behavior of Rectangular Hollow Steel Columns. *Journal of Structure Mechanic Earthquake Engineering* JSCE 2000; **647**: 79 – 95.
3. Aoki T, Ohnishi A, Suzuki M. Experimental Study on the Seismic Resistance Performance of Rectangular Cross Section Steel Bridge Piers Subjected to Bi–directional Horizontal Loads. *Journal of Structure Mechanic Earthquake Engineering* JSCE 2007; **63**(4): 716–726.

DOI: 10.1002/eqe

4. Goto Y, Jiang K, Obata M. Hysteretic Behavior of Thin–walled Stiffened Rectangular Steel Columns under Cyclic Bi–directional Loading. *Journal of Structure Mechanic Earthquake Engineering* JSCE 2007; **63**(1): 122−141.
5. Hayakawa R, Kawashima K, Watanabe G. Effect of bilateral loadings on the flexural strength and ductility of reinforced concrete bridge columns. *Journal of Structure Mechanic Earthquake Engineering* JSCE 2004; **759**: 79−98.
6. Ogimoto H, Kawashima K, Watanabe G, Nagata S. Effect of bilateral excitation on the seismic performance of reinforced concrete bridge columns based on hybrid loading test. *Journal of Structure Mechanic Earthquake Engineering* JSCE 2005; **801**: 33−50.
7. Nagata K, Watanabe E, Sugiura K. Elasto – plastic response of box steel piers subjected to strong ground motions in horizontal 2 directions. *Journal of Structure Engineering* JSCE 2004; **50**: 1427–1436.
8. Goto Y, Koyama R, Fujii Y, Obata M. Ultimate state of thin–walled stiffened rectangular steel columns under bi–directional seismic excitations. *Journal of Structure Mechanic Earthquake Engineering* JSCE 2009; **65**(1): 61–80.
9. Okazaki S, Usami T, Kasai A. Elasto–Plastic dynamic analysis of steel bridge piers subjected to bi–directional horizontal earthquakes, *Journal of Earthquake Engineering* JSCE 2003; **27**: 1–8.
10. Tsuboi H, Torii J, Kasai A, Usami T. The seismic design method for pipe–section steel bridge piers subjected to bi–direction horizontal earthquake motions, *Journal of Earthquake Engineering* JSCE 2007; **29**: 529–538.
11. JSCE. The Working Group of Seismic Design Formed in the Subcommittee on New Technology for Steel Structures. Guild line of seismic design for steel bridge and new technology for seismic design. 1996.
12. Obata M, Goto Y. Development of 3D Pseudo–dynamic Experiment System for Bridge Piers and Columns. *Journal of Structure Mechanic Earthquake Engineering* JSCE 2004; **725**: 253−266.
13. Nagata S, Watanabe G, Kawashima K. Effect of P − Δ Action of Actuators in a Hybrid Loading Test. *Journal of Structure Mechanic Earthquake Engineering* JSCE 2005; (**801**): 197−212.
14. Saizuka K, Itoh Y, Kiso E, Usami T. A Consideration on Procedures of Hybrid Earthquake Responses Test Taking Account of the Scale Factor. *Journal of Structure Mechanic Earthquake Engineering JSCE* 1995; **507**: 179–190.

DOI: 10.1002/eqe